EGG-OECD-9168

TMI-2 Examination Results from the OECD/CSNI Program Volume 1

D. W. Akers - United States
G. Bart - Switzerland
P. Bottomley - Commission of the European Communities
A. Brown - Sweden
D. S. Cox - Canada
P. Hofmann - Federal Republic of Germany
S. M. Jensen - United States
H. Kleykamp - Federal Republic of Germany
A. J. Manley - United Kingdom
L. A. Neimark - United States
M. Trotabas - France

Published April 1992

Idaho National Engineering Laboratory
EG&G Idaho, Inc.
Idaho Falls, Idaho 83415

Prepared for the
U.S. Department of Energy
Three Mile Island Operations Office
Under DOE Contract No. DE-AC07-76ID01570

ABSTRACT

As part of the Three Mile Island (TMI) Accident Evaluation Program, samples from the damaged TMI Unit 2 reactor core were examined by various countries under the auspices of the Organization for Economic Cooperation and Development's Committee on the Safety of Nuclear Installations. Participating countries include Canada, France, the Federal Republic of Germany, Japan, Sweden, Switzerland, the United Kingdom, and the United States. Also, the Commission of the European Communities participated. This examination program allowed an international group of experts the opportunity to evaluate material from the damaged reactor, and provided the basis for achieving an international consensus on sample examination results. The numerous types of examinations performed provide information in areas such as material interactions and relocation mechanisms, the distribution of materials and fission products, peak temperatures, and oxygen potentials in the core. The results of these examinations have substantively improved the understanding of the specific conditions that existed during the TMI-2 accident, as well as provided data for the verification of results from smaller-scale severe fuel damage experiments.

EXECUTIVE SUMMARY

The Three Mile Island Unit 2 (TMI-2) reactor underwent a prolonged loss-of-coolant accident that resulted in severe damage to the reactor core. Under the resulting accident evaluation program, an international collaboration for examination of TMI-2 samples was initiated by the Organization for Economic Cooperation and Development (OECD) with the intention of developing a consensus of results and using capabilities to the maximum. Examination results from the various participating countries are documented in Appendices B through K (see Volume 2). The opportunity was also used to evaluate full-scale reactor damage in comparison to computer codes and severe-accident tests.

TMI-2 has provided unique information that may not be readily obtainable from smaller-scale experiments. However, comparison between the TMI-2 accident and severe damage seen at the Loss-of-Fluid Test (LOFT) Facility and the Power Burst Facility (PBF) show similarities in the distribution and behavior of core materials and fission products, suggesting the existence of a consistent pattern of core melt progression.

Partially metallic melts from control material, zirconium, and structural materials were found in the lower crust, consistent with their early liquefaction and relocation to form blockages beneath. Above the "metallic melt" region was a region consisting of high temperature $(U,Zr)O_2$ ceramic melt covered by a crust. The TMI-2 central core was molten long enough to completely liquefy all the engulfed material. Above the upper crust was a debris bed consisting of partially damaged fuel rods and some molten materials that probably relocated after the core was reflooded. Similar damage of liquified fuel rods, blockages, and debris beds were observed in the severe fuel damage that resulted from experiments conducted at PBF and LOFT FP-2.

The upper crust in TMI-2 consisted of ceramic melt with agglomerations of metallic melted structural elements (Fe,Ni,Sn) and control rod alloy (Ag,In). This structure may have been formed by percolation of the metals downward into the solidified/solidifying crust. Metallographic examinations and X-ray diffraction indicated that the central $(U,Zr)O_2$ ceramic melt exhibited regions

of single-phase solid solution and regions of uranium-rich and zirconium-rich oxides [cubic $(\underline{U},Zr)O_2$ phases and either tetragonal or monoclinic $(\underline{Zr},U)O_2$ phases]. Single-phase regions indicated where the $(U,Zr)O_2$ melt was rapidly quenched, whereas two-phase regions indicated slower cooling of other portions. These microstructures are consistent with reflood water directly quenching the outer ceramic melt, and with other inner regions taking much longer to cool. This is consistent with thermocouple data indicating elevated temperatures for several days.

The ceramic melt relocating to the lower plenum flowed over stainless steel lower vessel components (e.g., the flow distributor) without damaging these materials. The $(U,Zr)O_2$ melt, which has a melting point of 2810 K, contained (Fe, Cr) oxide spinel structures in the grain boundaries that could be liquid at temperatures below the melting point of the stainless steel (less than 1720 K), and these locations probably contained the last materials to solidify. The material at this point in its descent to the lower plenum may therefore have been transported as a two-phase solid-liquid mass, with the liquid spinel carrying some solidified $(U,Zr)O_2$.

The segregations of various elements observed in the previously molten regions provides an indication of the low temperature interaction and relocation of materials. Zr-Fe and Zr-Ni eutectic interactions (from 1220 K) resulted in the liquefaction of stainless steel cladding and Inconel spacer grids at temperatures up to 500°C with melting points at approximately 1720 K. These liquefaction processes have also been observed in severe fuel damage resulting from experiments conducted at CORA and LOFT FP-2. Zr-Al-O eutectic interactions can lead to liquefaction of Al_2O_3-B_4C poison rods surrounded by zircaloy cladding above approximately 1620 K. These materials were found in the central melt regions and in the solidified crust, implicating such reactions in the early failure of TMI-2 fuel assemblies containing poison rods. Moreover, fuel assemblies containing burnable poison rods suffered greater damage than adjacent assemblies with control rods.

Silver-zirconium eutectic interactions can also lead to the low temperature liquefaction of the zircaloy cladding above 1200 K, as observed in the LOFT FP-2 experiment, but very little of this type of material was

observed in TMI-2. The higher core pressures may have limited the extent of this interaction. Molten zircaloy also appears responsible for fuel liquefaction and extensive $(U,Zr)O_2$ ceramic melt formation during the accident; this can take place at temperatures as low as approximately 2000 K, with molten $(U,Zr)O_2$ requiring temperatures in excess of 2810 K.

An indication of the core oxygen potentials during the accident was also given. Metallic melts were commonly composed of Ag-In and Fe-Ni-Sn, while oxidized phases commonly contained U, Zr, Cr, and Fe. This indicates an oxygen potential of approximately -150 kJ/mole at 2273 K to -500 kJ/mole at 1473 K.

The examination of intact fuel assembly remnants from the periphery of the core indicates that severe damage was limited to the central and upper regions of the core. Some of the fuel elements examined, for example, did not experience temperatures above 800 K. Despite the severe damage to the core and the relocation of tons of melt to the lower plenum, TMI-2 demonstrated that such an accident can be terminated without the loss of integrity of either the reactor vessel or containment.

ACKNOWLEDGMENTS

We wish to express our appreciation to the many representatives of countries that contributed to the contents of this work. Their contributions are duplicated in full and can be found in Appendices B through J, which are located in Volume 2 of this document.

The following list shows the contributors from each country that participated in the OECD-CSNI Program:

Canada

P. J. Fehrenbach
R. Choubey
G. Grant
G. Delaney
L. Brown
D. Chen
D. A. Leach
D. J. Disney
F. C. Iglesias
N. A. Keller
J. R. Mitchell
A. H. Kerr

Federal Republic of Germany

S. J. L. Hagen
G. Schanz
A. Skokan
R. Pejsa

France

M. Robin
G. Le Marois
J. Duco

Sweden

G. J. McIntyre
C. Graslund

Switzerland

W. Buhrer
R. Restani
H. U. Zwicky

United Kingdom

S. Whillock
J. F. W. Thompson
R. Williamson
S. A. Beetham

United States

R. V. Strain
J. E. Sanecki

Commission of the European Communities

M. Coquerelle

CONTENTS

FIGURES

TABLES

TMI-2 EXAMINATION RESULTS FROM THE OECD/CSNI PROGRAM

1. INTRODUCTION

The Three Mile Island Unit 2 (TMI-2) pressurized water reactor underwent a prolonged loss-of-coolant accident on 28 March 1979 that resulted in severe damage to the reactor core. As a consequence of the TMI-2 accident, numerous aspects of light water reactor safety have been questioned, and the United States Nuclear Regulatory Commission (NRC) has embarked on a thorough review of reactor safety issues, particularly the causes and effects of severe core damage accidents. The nuclear community acknowledges the importance of examining TMI-2 in order to understand the nature of the core damage. Immediately after the accident, four organizations [General Public Utilities Nuclear Corporation (owner/operator of TMI), Electric Power Research Institute, the NRC, and the U.S. Department of Energy (DOE) collectively known as GEND] performed the initial postaccident evaluations of TMI-2. Under the auspices of the OECD's Committee on the Safety of Nuclear Installations, a number of OECD countries and the Commission of the European Communities' Joint Research Centre participated in the TMI-2 Accident Evaluation Program by performing detailed examinations of samples of fueled debris. This report describes the results of those examinations.

Participants who have completed examinations include Canada, the Commission of the European Communities Joint Research Centre, France, the Federal Republic of Germany, Sweden, Switzerland, the United Kingdom, and, in the United States, Argonne National Laboratory and Idaho National Engineering Laboratory. A shipment to Japan was completed in 1991, and results of its examiniation will be available by the Japan Atomic Research Institute. A broad spectrum of examinations performed by these countries are documented in the appendices of this report (see Volume 2). Examinations were performed on samples of debris collected from various regions within the reactor vessel. Examination of these samples has contributed new and valuable information for understanding the accident.

The end-state configuration of the TMI-2 core just after the accident as determined by closed circuit television (CCTV), mechanical probing, and core-boring operations[1] is illustrated in Figure 1. Current estimates indicate that approximately 19% of the original core mass formed an upper layer of debris supported by a hard crust.[2] Below the upper debris bed was a consolidated mass (approximately 25% of the total core mass) composed of an upper crust, peripheral or side crust of differing composition, a central core region of the consolidated mass, and a lower crust. Standing fuel rod segments were below the consolidated mass. A portion of the core mass (14%) had also flowed down onto the lower reactor vessel head. CCTV examinations of the debris deposited on the lower reactor vessel head were used to estimate the volume of deposited material.[3]

Much of the information on the distribution of materials in the core was obtained from a number of sampling and examination programs performed as part of the DOE-sponsored Accident Evaluation Program.[4,5] One of the principal sources of information on the lower core region was the core sampling operation that was performed in July 1986.[6,7] The core boring operation was performed using a specialized computer-controlled, electromechanical device based upon commercial core drilling equipment from the mining/geology industry. From these sampling operations, a variety of loose debris samples were obtained from the upper core loose debris bed, the central core region (crusts and debris bed), and the material that relocated to the lower head of the reactor vessel.

M. L. Russell[8] and others have provided summaries of the TMI-2 Accident Evaluation Program, including examinations performed and principal results. Preaccident operations, original core materials, and fission product distributions have been discussed at length.[9,10,11]

The remainder of this report discusses the objectives of the OECD-CSNI examination program, the samples examined as part of the program, a brief description of core melt progression phenomenology, a discussion of the examination results, and the significance of these results as related to the TMI-2 accident and small-scale severe accident tests such as the LOFT program.

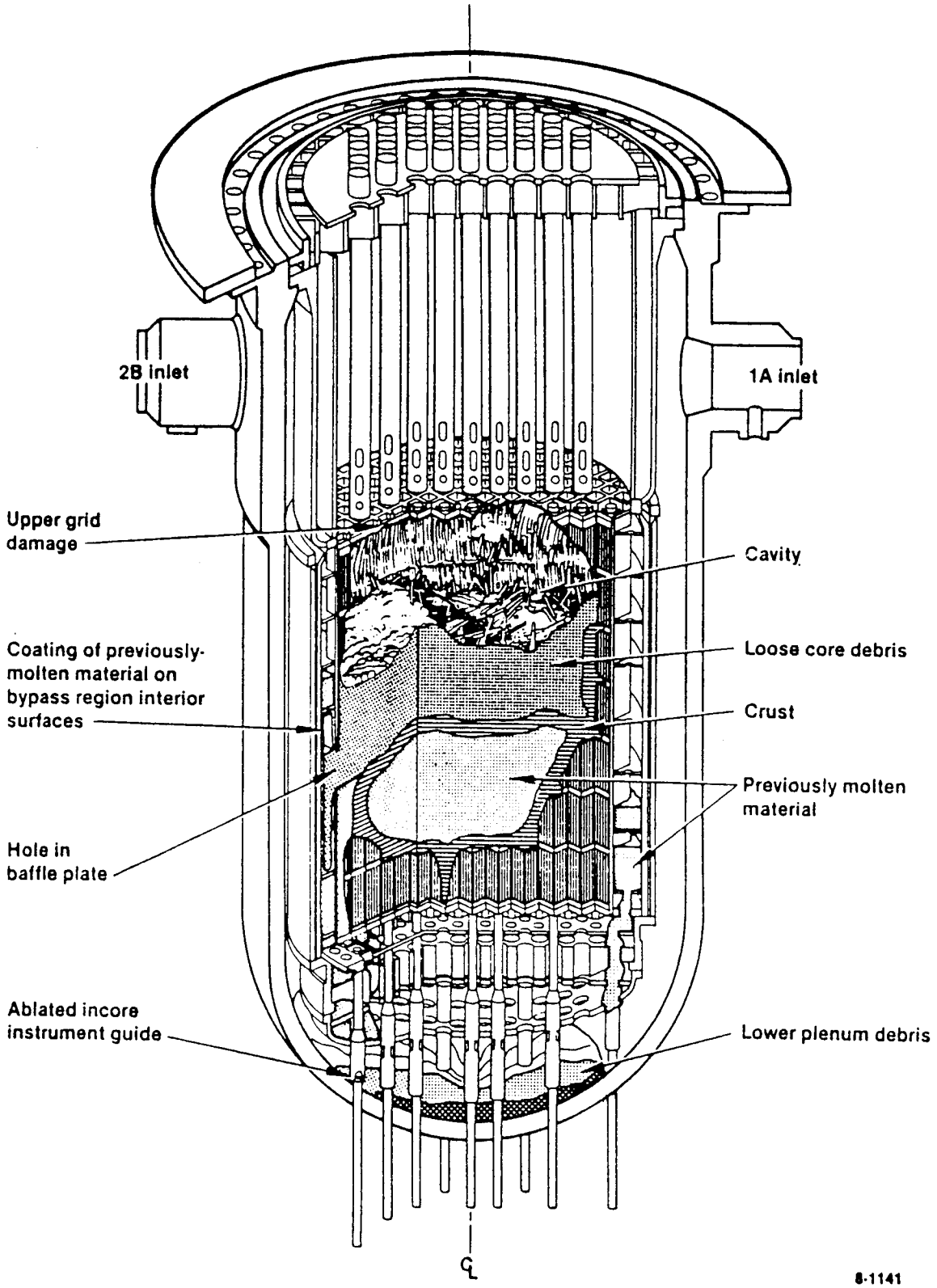

Figure 1. TMI-2 core end-state configuration.

2. EXAMINATION OBJECTIVES

The general objectives of the examination of TMI-2 samples by the international participants in the OECD-CSNI examination program are to develop an international consensus on the results of the TMI-2 samples and to utilize international capabilities to obtain as much information as possible on severe accident materials behavior from the examinations. Specific objectives of the individual examination programs are

- To understand the end-state condition of the TMI-2 core through physical, metallurgical, chemical, and radiochemical examinations, and to assess the external influences that resulted in the observed phenomena
- To assess what happened during the accident and to provide information useful for benchmarking severe accident analysis codes
- To define the relationship between the phenomena and processes controlling the accident and the important severe accident/source term technical issues.

Examinations performed by the various countries include a wide variety of techniques and analysis methods, many of which were not available to the DOE TMI-2 Accident Evaluation Program. Examinations performed include:

- Physical morphology of the debris (weight, density, and porosity)
- Material properties (optical evaluation, microprobe, x-ray, and neutron diffraction)
- Composition and chemical form (if possible) and the peak temperatures to which those materials were exposed
- Distribution and retention of radionuclides in the debris.

These examinations performed by participating laboratories provide extensive data for assessment by a number of experts and a forum for the development of an international consensus on these data.

3. SAMPLE DESCRIPTION

Various locations of the TMI-2 reactor vessel were sampled, each sample beginning at the top and continuing vertically down through the reactor vessel to the lower head (see Figure 1 on page 3). These samples include sections of partial fuel and control rods, prior molten debris from the upper core loose debris bed, sections of crusts from the central core region, and the debris that relocated to the lower head of the reactor vessel. Table 1 lists the types of samples examined and the countries that performed those examinations. A list of the individual samples examined is shown in Appendix A.

Table 1. OECD-CSNI sample examinations

Particpant	Samples				
	Core bores	Fuel rod segments (peripheral)	Fuel assembly rod segments and control rods	Upper core loose debris	Lower core loose debris
Canada	X	X	X	X	X
Commission of the European Communities	X	X	X	X	--
France	X	X	X	X	X
Federal Republic of Germany	X	X	X	--	X
Sweden	X	--	--	--	X
Switzerland	X	--	--	--	--
United Kingdom	X	X	X	--	X
United States Nuclear Regulatory Commission	X	X	--	X	--

4. CORE MELT PROGRESSION PHENOMENOLOGY

This section provides a brief summary of the significant phenomena that may occur during a severe core damage accident for comparison with the examination results discussed in the next section. A detailed discussion of these phenomena[12] is provided in Appendix B, but the following summary should provide a background for understanding the results from the examination of TMI-2 samples.

4.1 Initial Uncovery

Upon core uncovery, the core will begin to heat up as a result of decay heat. Above approximately 1070 K, the Ag-In-Cd control material will melt within its stainless steel cladding. As temperatures continue to increase due to decay heat and the exothermic oxidation of zircaloy and stainless steel components, Fe-Zr and Ni-Zr eutectic interactions may occur between the stainless steel control rod cladding and the surrounding zircaloy guide tubes at temperatures above approximately 1220 K. This could result in the failure of the stainless steel cladding and the release of the molten Ag-In-Cd control material. The molten control material may be initially released as an aerosol or a liquid, depending upon the pressures within the core when rod failure occurs. The control material can begin to liquefy the zircaloy cladding above approximately 1470 K as a result of Ag-Zr eutectic interactions. Above this temperature regime, the rapid oxidation of zircaloy and stainless steel become important factors because of the heat generated by these exothermic interactions. These interactions may lead to rapid temperature escalations, which would result in the melting of the stainless steel cladding and Inconel spacer grids above approximately 1720 K, and ultimately the melting of unoxidized zircaloy above approximately 2030 K. Melting of the stainless steel and Inconel components could lead to further zircaloy liquefaction as a result of the aforementioned Fe-Zr and Ni-Zr eutectic interactions. An additional phenomenon that occurs in this temperature regime is the failure of the Al_2O_3-B_4C burnable poison rods due to Al-Zr eutectic interactions between the poison material and the surrounding zircaloy cladding. This can occur as low as approximately 1620 K.

The zircaloy oxidation kinetics will depend upon the steam availability, but typically a ZrO_2 oxide layer will form on the outer surface of the cladding, under which will be a partially oxidized alpha-Zr(O) layer, with unoxidized metallic zircaloy on the cladding inner surface. The relative melting points of these materials are 2960 K for the ZrO_2, approximately 2300 K for the alpha-Zr(O), and 2030 K for the unoxidized zircaloy. As temperatures in the core continue to increase, the metallic zircaloy on the cladding inner surface will be the first of these materials to melt. This molten zircaloy may be contained by the outer oxidized layers, allowing the molten zircaloy to interact with the UO_2 fuel forming a (U,Zr,O) melt. As a result, fuel liquefaction may begin at temperatures well below the 3120 K melting point of the fuel. With adequate steam availability and temperatures, ceramic $(U,Zr)O_2$ melts may exist above approximately 2800 K, resulting in extensive material relocation and core damage.

These material interactions result in the relocation and solidification of various materials at different times and places throughout the core. However, similarities exist between the post-test stratification of material in in-pile severe fuel damage tests and the damaged TMI-2 core.[13,14] In all cases a metallic melt region is found near the bottom of the damaged region, which is formed as a result of the early liquefaction and relocation of control rod and structural materials. In many cases, this material solidifies at or near a spacer grid location, forming a partial blockage that can divert or redirect any subsequent steam flow. A ceramic blockage region consisting of $(U,Zr)O_2$ [or possibly (U,Zr,O), depending upon steam availability] typically forms above the metallic blockage. Both the metallic and ceramic blockages consist of previously molten material surrounding the remnants of the fuel rod array. Above the ceramic melt region, a debris bed of fuel pellets, cladding remnants, and other partially damaged core components is typically found.

4.2 Rapid Oxidation

The exact post-test or post-accident condition will be greatly influenced by such factors as steam availability and the extent of damage prior to reflood. Steam availability will influence the heatup rate because of the importance of the zircaloy/steam reaction (see Appendix B). At slow heatup

rates (less than 0.5 K/s), the zircaloy cladding can be completely oxidized before reaching the melting point of metallic zircaloy. In this case, molten zircaloy is not available to cause liquefaction of the fuel until temperatures exceed 2800 K. At intermediate heatup rates from 1-5 K/s, molten zircaloy may be held adjacent to the fuel by an outer oxide layer, resulting in the liquefaction of fuel at temperatures as low as approximately 2000 K. At fast heatup rates (greater than 5 K/s), the outer zircaloy oxide layer may be too thin to restrain molten zircaloy on the cladding inner surface, and in-situ fuel liquefaction may be limited because of the rapid relocation of molten zircaloy through a breach in the oxidized shell.

4.3 Reflood

The timing of reflood may have contributed to the extensive damage to the upper core region. Also, the reflood stage can have a profound effect on the extent and timing of hydrogen generation during a severe core damage accident. In the Loss-of-Fluid Test Facility (LOFT) LP-FP-2 severe fuel damage test (see Reference 13), relatively large amounts of metallic zircaloy were above or near the melting point when reflood occurred.[15-20] Conditions in the bundle went from nearly steam-starved to steam-rich almost instantaneously, resulting in the rapid oxidation of the hot metallic zircaloy, leading to an end-state configuration similar to TMI-2. It was observed that temperature escalation in the fuel bundle and the generation of large amounts of hydrogen are associated with this phase of the accident.

Despite the complex and interactive processes that may occur during a severe core damage accident, the results of a multitude of experiments indicate a consistent pattern of certain basic phenomena. The examinations of sample materials from the TMI-2 reactor core provided evidence of the similarity of physical and chemical phenomena identified in separate-effects tests and out-of-pile and in-pile severe fuel damage experiments with the TMI-2 accident.

5. SUMMARY OF EXAMINATION RESULTS

A variety of examinations were conducted on samples from throughout the TMI-2 reactor core. These examinations included visual examinations, density measurements, metallography, scanning electron microscope/microprobe examinations, secondary ion mass spectroscopy (SIMS), X-ray diffraction, and neutron diffraction. All of these examination techniques complement each other and provide data with which to more fully understand the complex material interactions that occurred in TMI-2. The agreement in the results obtained by several different analysts provides confidence that these results accurately describe the various phenomena that occurred during the TMI-2 accident. The results of these examinations are summarized in the following sections, with individual papers describing the detailed results provided in Appendices C through K. These papers are also listed as References 21 through 27 and Reference 29.

5.1 Density Measurements

Immersion density measurements were conducted on samples from several different regions of the core. These are summarized in Table 2. Most of the data are for previously molten material from the central core region. Densities in this region varied from 6.70 to 8.68 g/cm^3, with an average density of 7.71 g/cm^3. The density of lower plenum sample, 11-1-A (8.19 g/cm^3), was very similar to the densities of materials from the central molten region, which is consistent with the hypothesis that this material originated in the central core region. The density of the sample from the lower crust was relatively low, 6.7 g/cm^3, which reflects the ferrous metal content of samples from this region. These results are comparable to density measurements that were conducted on a multitude of similar samples at the INEL (see Reference 7). The large ranges in densities can be attributed to differences in composition and porosity.

5.2 Metallurgical Examinations

This section summarizes the results of the metallurgical examinations. These examinations included optical metallography to characterize the samples,

Table 2. Density measurements

Core Location	Sample	Density (g/cm^3)	Reference
Intact rods	C7-3-35	9.03	P. Bottomley et al.
Upper debris	H8-7	7.14-9.83	P. Bottomley et al.
Central	G12-P2-E	7.38	P. Bottomley et al.
	G12-P6-E	7.45	P. Bottomley et al.
	G12-P9-B	7.12	P. Bottomley et al.
	G12-P10-A	8.68	P. Bottomley et al.
	G8-P4-A-1	7.84	H. Kleykamp et al.
	G8-P4-A-2	7.77	H. Kleykamp et al.
	G12-P10-C	7.29	H. Kleykamp et al.
	K9-P4-C	6.70	H. Kleykamp et al.
	N5-P1-B	8.31	H. Kleykamp et al.
	O7-P3-O	7.82	H. Kleykamp et al.
	K9-P3-M	8.50	M. Trotabas et al.
	G8-P8-C	8.34	G. Bart et al.
Lower crust	N5-P1-E	6.70	P. Bottomley et al.
Lower plenum	11-1-A	8.19	H. Kleykamp et al.

scanning electron microscope/microprobe analyses to assist in identifying the phases resulting from various material interactions, and X-ray and neutron diffraction to identify chemical compounds and crystal structures. These examinations provided data on the material interactions that occurred, the redistribution of materials, the extent of oxidation in the core, and estimates of peak temperatures reached in various regions of the core.

5.2.1 Intact Fuel Rod Segments

Several sections of intact fuel rod remnants were examined at various examination facilities (see Table 1 on page 5). These fuel rod segments were still contained within the upper portion of the respective fuel bundle assemblies, so that their core location could be identified. The bottom-end tips of these rod segments were typically broken off--either as a result of

damage during the accident or possibly from subsequent handling. In all cases, the damage to the remaining rod segments was minimal, with only minor amounts of surface oxidation on the zircaloy cladding, and minor amounts of zircaloy hydriding noted in some instances. No evidence of gross overheating was observed on any of the segments, with estimates varying from less than 800 K to temperatures slightly above 1230 K, based upon the cladding microstructure and estimates of oxygen diffusion rates to form the surface oxide layers. The observed variations may be attributed to different core locations and varying axial locations.

The fuel structure was unaffected, except that some fuel "desintering" was noted in one case as a result of zircaloy interactions with the fuel (see Appendix C).[21] The fuel grain size was 5-15 μm, with no evidence of fuel grain growth or restructuring. Oxygen/metal fuel measurements indicated that no oxidation of the fuel took place in these core locations.

These observations indicate that portions of fuel assemblies on the periphery of the core were not heavily damaged during the accident, and that the major damage was limited to the central portion of the core.

5.2.2 Upper Crust

Six samples from the upper crust were examined by various participants. In all cases, the samples were characterized as agglomerates of separate ceramic and metallic phases. The metallic melts penetrated along cracks in the $(U,Zr)O_2$ ceramic matrix material, and metallic phases also precipitated from the ceramic melt region. This morphology suggests that metallic melts may have flowed down from above and penetrated along cracks in the solidified ceramic upper crust.

Metallographic and SEM (scanning electron microscopy)/microprobe examinations indicated that separate uranium- and zirconium-rich phases of $(\underline{U},Zr)O_2$ and $(\underline{Zr},U)O_2$ were present in the ceramic matrix, as well as small amounts of spinel material within the grain boundaries of the ceramic melt. The spinel type structure (AB_2O_4) was identified from X-ray diffraction (see Appendix D),[22] and SEM/microprobe analyses further identified the presence of

Fe-Cr-O, which may exist as a spinel (see Appendices E and F).[23,24] SEM/microprobe examinations further indicated that the uranium- and zirconium-rich phases each contained less than 10 wt% of the solute atom, and that X-ray and neutron diffraction revealed the presence of the cubic type UO_2 structure and both monoclinic and tetragonal ZrO_2. These phases can be understood by examining the UO_2-ZrO_2 phase diagram in Figure 2, which shows that upon cooling, the melt should first form a single-phase solid solution of $(U,Zr)O_2$, but that upon further cooling under equilibrium conditions, this solid solution should decompose into a two-phase structure consisting of cubic $(\underline{U},Zr)O_2$ and tetragonal $(\underline{Zr},U)O_2$. Additional slow cooling beyond this point should result in the formation of cubic $(\underline{U},Zr)O_2$ and monoclinic $(\underline{Zr},U)O_2$. The two-phase structures therefore indicate that at least some of this material cooled slowly enough to allow the formation of these separate phases, and were not rapidly quenched to the extent that the $(U,Zr)O_2$ solid solution phase was retained. This is consistent with thermocouple data, which indicate that the core remained hot for an extended period of time following the accident.

Several different families of metallic melts were generally observed among all the investigators. These metallic melts were also observed in other regions of the core, indicating a general propensity for these elements to group together. Although small amounts of other elements were commonly mixed in these phases and were reported to various extents, a general pattern was apparent. These groupings of metallic melts are described below.

Control rod materials were predominately precipitated as separate phases. Silver and indium were always found together; in most cases, however, the cadmium was no longer present, or was greatly diminished in relation to the as-fabricated control rod alloy (80 wt% Ag, 15 wt% In, 5 wt% Cd). This is attributed to the higher volatility of cadmium. Tin was also commonly observed with the control rod materials.

Iron, nickel, and tin were commonly observed together. Sometimes the phases were reported as containing all three elements, and sometimes phases of only Fe-Ni or Ni-Sn were reported. In the latter cases, it is possible that the third element, as well as other minor constituents, may have been present in relatively small quantities, but were not specifically reported by the

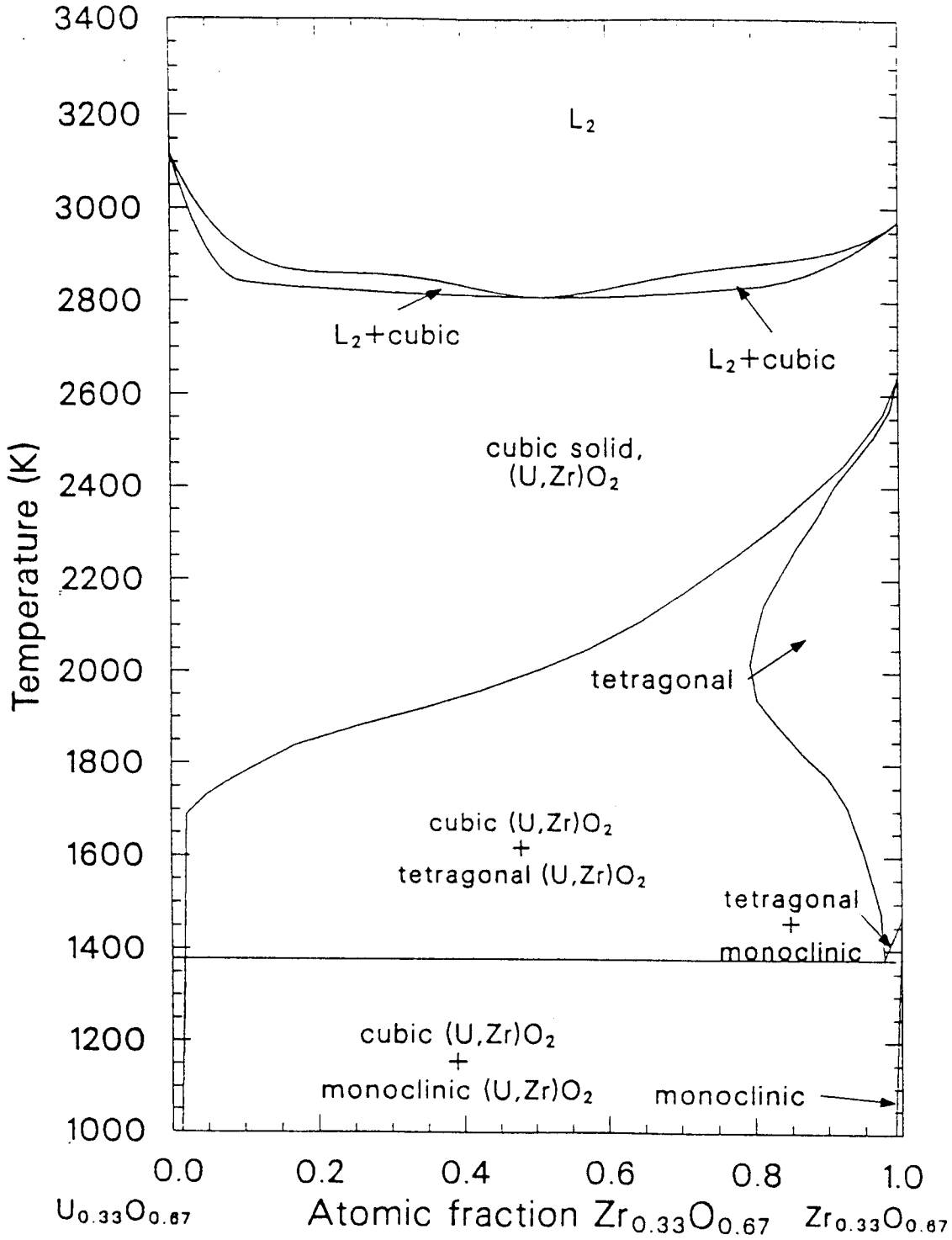

Figure 2. UO_2-ZrO_2 pseudobinary phase diagram.

author. However, this type of metallic phase was found in all six upper crust samples examined by all investigators. G. Bart (see Appendix E) found Ni-Sn phases containing approximately 40% Sn, which suggests the possible existence of Ni_3Sn_2 precipitates that form below 1500 K. Neutron diffraction also indicated the presence of gamma-(Fe,Ni), which would precipitate below approximately 1700 K. M. Trotabas (see Appendix D) indicated the presence of the fission product ruthenium in a Ni-Fe-Sn metallic melt.

Chromium was observed as a minor component in some of the metallic phases (see Appendix E); in general, however, it seemed to form oxidized spinel structures of Fe-Cr-O. This is consistent with the fact that chromium oxidizes very easily; consequently, only small amounts trapped in molten stainless steel or Inconel would be expected to remain metallic.

The presence of Ag, In, Ni, and Sn in the metallic state; Fe in both the metallic and oxide states; and Cr generally as an oxide provides some indication of the oxygen potential during the accident. As shown in the Ellingham diagram in Figure 3 (see Appendix G),[25] above the temperature range from 1200-2000°C (1473-2273 K), the likely range of oxygen potentials are between approximately -150 kJ/mole (Sn/SnO_2 equilibrium at 2000°C) and -500 kJ/mole (Cr/Cr_2O_3 equilibrium at 1200°C).

5.2.3 Central Molten Region

Samples from this region were primarily $(U,Zr)O_2$ ceramic melt, with only minor amounts of metallic phases within the ceramic matrix. The ceramic melt contained regions of uranium- and zirconium-rich phases, with $(Fe,Ni,Cr,Al)O_4$ spinels similar to those found in the upper crust and lower plenum samples. X-ray diffraction confirmed that the cubic $(U,Zr)O_2$ structure was present, as well as both tetragonal and monoclinic $(Zr,U)O_2$ structures. This suggests that at least parts of these samples were cooled slowly enough to allow the $(U,Zr)O_2$ solid solution to decompose into the separate $(U,Zr)O_2$ and $(Zr,U)O_2$ phases. In other areas, however, the solidified melt consisted of a single phase amorphous $(U,Zr)O_2$ structure, which suggests that these portions were rapidly quenched to the extent that the $(U,Zr)O_2$ solid solution was frozen in place.

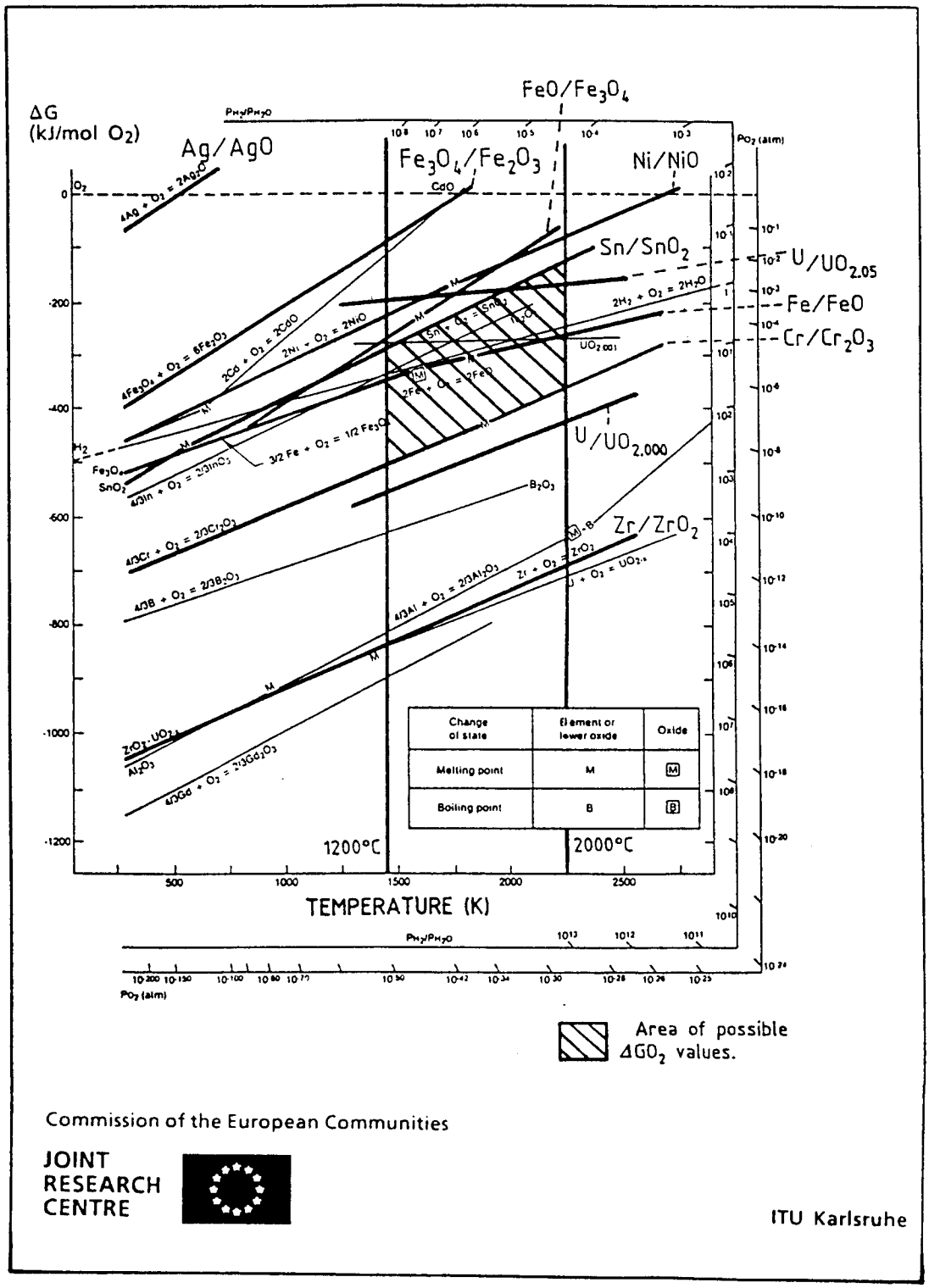

Figure 3. Standard free energy (DG) diagram for the main TMI-2 core materials and their oxides showing the likely range of oxygen potentials existing in the agglomerate zone during the accident (as inferred from sample examination).

The metallic phases were predominately Fe-Ni-Sn (with minor amounts of chromium sometimes indicated) and silver-rich melts (usually with indium also present). Metallic spheres of silver precipitate were sometimes noted (see Appendix G). In another instance, an Ag(In,Cd,Sn) melt was observed in which $Ni_3(Sn,In)_2$ had precipitated out as dendrites (see Appendix H).[26] This compound has a melting point of 1537 K. These metallic phases were similar to those found in the upper crust, but fewer of these materials were present in the central melt region. These metallic phases tended to be located around voids, as opposed to large veins of melt as were observed in the upper crust. This suggests that the voids formed adjacent to the last material to solidify--the lower-melting-point metallic phases. Large veins of metallic melt were not observed, as they were in the upper crust, because metallic melts were not flowing over a solidified ceramic crust. Complete mixing occurred because the material in this region was a high temperature molten mass.

X-ray diffraction by several investigators confirmed the presence of the cubic $(\underline{U},Zr)O_2$ structure, tetragonal and monoclinic $(\underline{Zr},U)O_2$, and a cubic spinel structure (see Appendix I).[27] (Also see Appendices D and G.) Neutron diffraction measurements (see Appendix E) indicated a lattice parameter for the tetragonal $(\underline{Zr},U)O_2$ structure, which corresponded to 90% ZrO_2 and 10% UO_2. This was confirmed by energy-dispersive X-ray spectroscopy measurements on the same sample that indicated uranium- and zirconium-rich phases with less than 10% solute. Based upon the UO_2-ZrO_2 phase diagram in Figure 2, this suggests a thermal hold near approximately 1750 K to precipitate these phases, and the length of this hold was estimated to be from 3-72 hours based upon grain sizes from 1-5 μm (see Appendix E). Similar microprobe results were noted by Bottomley (see Appendix G), who found uranium- and zirconium-rich oxide phases containing a few at.% of solute, and grain sizes from 1-10 μm. Brown (see Appendix I) also measured changes in the lattice parameters of $(\underline{U},Zr)O_2$ and $(\underline{Zr},U)O_2$ structures, which could be accounted for with solute concentrations of less than 10 mole%, assuming stochiometry. It was noted in this same study that the observed changes in the lattice parameters might be attributed to hyperstochiometry; however, it was noted that there was no diffraction pattern indicating the presence of U_3O_8.

Aluminum was identified in the spinel phase, which was not identified in the spinels in the upper crust. As described in the following section, aluminum was also found in the lower crust. This suggests that the Al_2O_3-B_4C burnable poison rods melted relatively early in the accident and flowed downward prior to the formation of the upper crust. This early melt relocation may be due to interactions between the Al_2O_3 and the zircaloy cladding surrounding these rods, resulting in the formation of a Zr-Al-O low temperature melt. Investigations have shown (see Appendix B) that such interactions can lead to the onset of liquefaction at approximately 1350°C (1623 K). Other examinations have indicated that the fuel assemblies containing burnable poison rods showed increased damage[28] (72 of the 177 fuel assemblies contained 16 burnable poison rods), as evidenced by greater damage to the remaining upper-end fitting in adjacent assemblies containing control rods and burnable poison rods.

5.2.4 Lower Crust

Samples from the lower crust region generally consisted of intact fuel pellet stacks surrounded by metallic melts. In some cases, remnants of the oxidized cladding shells surrounded the fuel pellets; in other cases, however, the cladding was no longer present. The metallic melts consisted of control rod alloy mixed with tin (Ag,In,Cd,Sn) and structural materials; reported metallic phases included (Ni,Sn,Fe), (Zr,Fe), (Fe,Ni,Cr,Al), (U,Zr,O), and (Zr,Fe,Cr,Ni). Small amounts of oxide phases were also observed; reported phases included $(U,Zr)O_2$ adjacent to the fuel, Cr_2O_3 spheres that were immiscible with silver-rich metallic melts, and Ni-Cr-Fe-oxides, as well as UO_2 fuel and ZrO_2 oxidized cladding containing small amounts of iron and nickel.

The majority of the metallic melt consisted of molten structural materials, with iron being the predominant element. One analysis (see Appendix G) found typical concentrations of [(66 at.% Fe)-(33 at.% Ni)]. Ni-Sn precipitates were also typically found in grain boundaries, probably as Ni_3Sn_2, with minor amounts of indium and iron sometimes reported (see Appendices G and H).

Control rod materials generally precipitated as separate phases within the metallic matrix. These phases were rich with silver and contained significant amounts of indium, but the cadmium was depleted in relation to the original control rod alloy (80 wt% Ag, 15 wt% In, 5 wt% Cd). One analysis (see Appendix H) reported (88 wt% Ag, 10 wt% In, 1 wt% Cd, 1 wt% Sn) on one sample, and silver-rich material containing up to (18 wt% In) on another sample.

X-ray diffraction indicated the presence of the UO_2 cubic structure with a decreased lattice parameter due to Zr solute atoms in the solid solution (see Appendix H). Monoclinic ZrO_2 with a larger lattice parameter was also found, which was attributed to the presence of Fe and Ni in the ZrO_2. This analysis also confirmed the presence of the hexagonal Ni_3Sn_2 phase containing minor amounts of indium, cadmium-depleted control rod material, gamma-Fe-Ni-Cr, and some molybdenum-based alloys.

5.2.5 Lower Plenum Samples

Samples from the lower plenum were generally composed of ceramic $(U,Zr)O_2$ melt material, similar to samples from the central molten core region. This suggests that molten material contained in the central core region was released through a breach in the surrounding crust, and that this material flowed downward and eventually solidified in the lower plenum. Phase segregation into $(\underline{U},Zr)O_2$ and $(\underline{Zr},U)O_2$ was observed, although in other areas of these samples, the microstructure was characteristic of a single-phase solid solution of $(U,Zr)O_2$. This indicates that portions of these samples were quenched quickly enough to retain the high-temperature solid-solution phase, whereas other portions of these samples cooled more slowly and enabled the two-phase structure to develop. This may be explained by molten material suddenly coming into contact with water near the bottom of the core, rapidly quenching at least some of the material. A spinel structure was located in the grain boundaries, which may have been liquid at temperatures below the melting point of stainless steel (~1700 K). This would have allowed for mass transport of material to the lower plenum in the form of a two-phase solid-liquid slurry. This would account for the fact that this material flowed over the stainless steel diffuser plate and the stainless steel liner covering the lower vessel head without damaging these materials. This

contrasts with the ablated outline of the certain reactor structures higher up, which appear to have been in contact with fully molten corium.

Neimark observed rounded grains of single-phase $(U,Zr)O_2$ indicative of material that had been rapidly cooled from the liquid state, with additional phases in the grain boundaries (see Appendix J).[29] The grain boundary phases included uranium- and zirconium-rich phases. In addition to this basic microstructure, eutectic structures were observed near gas bubble voids in some samples. These eutectic structures consisted of $(\underline{U},Zr)O_2$, $(\underline{Zr},U)O_2$, and Fe-Al-Cr-Ni oxide spinels. The presence of these low-melting-point phases near gas-containing voids further indicates that these were the last areas to solidify. Similar structures were also found by Kleykamp (see Appendix H) and Olsen.[30]

X-ray diffraction measurements (see Appendix I) also indicated that portions of the samples consisted of a single-phase solid solution of $(U,Zr)O_2$ as evidenced by large line broadening effects and large decreases in the lattice parameter, indicating a more rapid cooling of the structure. However, these same studies also found evidence of the tetragonal $(Zr,U)O_2$ structure and lesser amounts of the lower temperature monoclinic $(Zr,U)O_2$ structure. Similar analysis on other samples (see Appendix H) showed similar results, with cubic $(\underline{U},Zr)O_2$ and tetragonal $(\underline{Zr},U)O_2$ structures of compositions $U_{0.9}Zr_{0.1}O_2$ and $Zr_{0.86}U_{0.14}O_2$. The presence of these two-phase structures indicates that this material cooled slowly.

5.2.6 Upper Core Debris

Debris samples from the region on top of the upper crust were also examined (see Appendix G). These examinations found a variety of materials that had experienced some form of damage, including oxidized cladding remnants, fuel with metallic Fe-Cr-Ni along grain boundaries, control rod cladding remnants, and some metallic and ceramic melts. These materials represent material that relocated relatively late in the accident, after the solidification of the upper crust and probably continuing into the reflood stage.

5.3 Characterization of Fission Products

Most of the participants in the program performed fission product examinations by using both standard radiochemical techniques and more exotic methods such as fission gas analysis (see Appendix G), SIMS (see Appendix E), and gamma ray mapping techniques (see Appendix C). The examinations performed, including those performed using standard techniques, have provided new information on radionuclide transport and behavior in the TMI-2 reactor core.

Examinations of TMI-2 core debris for radionuclide content were performed on more recent samples of debris from near the lower head of the reactor vessel (see Appendix K). These examinations indicate that the samples of material near the lower head of the reactor are similar in composition to material in the central core region. All radiochemical examination results tend to verify the earlier work discussed in References 7 and 8.

Examinations performed by Bottomley (see Appendix G) for fission gas analysis indicated that no volatile fission gases had been retained in the melt and that volatile radionuclides such as Cs-137 were retained in the melt despite high temperatures. Examinations indicated that these volatile fission products were retained in the melt at temperatures up to 2000°C and that substantial releases occurred at temperatures of 2500°C [temperatures near the melting point of the $(U,Zr)O_2$ melt]. Releases at this temperature were indicated for all radionuclides, including low volatile fission products such as cerium and europium.

Examinations by Bart using SIMS techniques indicated a number of correlations between various fission products and various material phases present in the material. Specific observations of importance are that the radionuclides of Mo, Ru, and Tc are correlated among each other and with Fe and Ni. Therefore, noble fission metals can be expected to concentrate in metallic phases and would be expected to be primarily concentrated in the crust regions and in metallic inclusions in the core.

As previously indicated in the metallurgical section, metallic material tends to concentrate in a secondary phase around voids, and previous work based on autoradiographs (see Appendix J) suggests that there is a significant accumulation of beta- and gamma-active materials at these points in the samples.

Another important observation is that the rare earth fission products La, Pr, Ce, Nd, and Pm are more significantly correlated with Zr than with U, which suggests that these lanthanides may prefer, as host lattice, the Zr-rich tetragonal $(\underline{Zr},U)O_2$ phase rather than the cubic phase. Further, there are apparent correlations between the Sr and the Zr phases, which indicates that this relatively low volatility radionuclide is mobile and tends to move to zirconium-rich phases.

Of particular importance in Bart's work is the lack of fission product correlations with Ag, In, and Sn. These data suggest that none of the radionuclides (particularly tellurium) tend to concentrate in the Sn phases. This helps understand tellurium behavior because one of the stable chemical forms is tin telluride.

Examinations by Cox (see Appendix C) indicate that the peripheral and lower intact fuel samples examined retained their intact fission product inventories, which suggests that much of the decay heat was retained within the core and that releases from the partial assemblies did not occur.

Trotabas et al. (Appendix D) observed volatile fission products on the outer surface of the fuel rod cladding, pointing to condensation of such elements on cooler surfaces, even with the reactor.

6. SIGNIFICANCE OF DATA OBTAINED FROM THESE EXAMINATIONS

Similarities between experimental test results and the phenomena observed at the TMI-2 accident indicates that there is a consistent pattern of in-core damage progression, which is determined by the physical and chemical properties of the core materials. However, the examination of samples from the TMI-2 reactor has provided a unique opportunity to study these interactions in a full-sized reactor, not only confirming the validity of the experimental observations, but also providing some unique information that may not have been readily apparent from the smaller scale experiments. The data from TMI-2 are therefore useful in understanding severe fuel damage accidents in a general sense, as well as providing a better understanding of the specific phenomena that occurred during the TMI-2 accident. This section discusses some of the contributions that these sample examinations had on understanding the TMI-2 accident and severe fuel damage accidents in general.

The general stratification of relocated material following the TMI-2 accident was similar to that observed in experiments (see References 13 and 14). Partially metallic melts containing control material, zirconium, and structural materials were found in the lower crust, consistent with the early liquefaction and relocation of these materials. These "metallic melts" completely surrounded the remaining fuel rod array and were very similar to the metallic lower blockage regions observed in experiments. Above the metallic melt region was a region consisting of high temperature $(U,Zr)O_2$ ceramic melt surrounded by a solidified crust of similar material. In the case of TMI-2, this molten material remained hot enough for a sustained period of time to completely liquefy all the material in the central region. In the severe fuel damage 1-4 (see Reference 14) and LOFT FP-2 experiments (see Reference 13), the ceramic melt was able to partially liquefy some of the material in this region, but significant amounts of the original fuel rod array were still present. The differences simply reflect different stages of damage progression. Above the solidified ceramic upper crust was a debris bed consisting of partially damaged fuel rods and some molten materials that probably collapsed from above after the core was reflooded. Similar debris beds were observed in the severe fuel damage experiments conducted in PBF, as well as the LOFT FP-2 experiment.

The upper crust in TMI-2 consisted of ceramic melt with agglomerations of metallic melt in voids and cracks in the ceramic matrix. This suggests that these metallic melts flowed downward and penetrated into the solidifying crust. These metallic melts were predominantly mixtures of structural elements (Fe,Ni,Sn) and control rod alloy (Ag,In). Cadmium was generally depleted in relation to the other control rod elements due to its high volatility. This solidified melt morphology indicates that structural and control rod materials continued to be liquid in the upper portion of the core after the higher temperature ceramic melt portions of the upper crust had solidified.

Metallographic examinations indicated that the $(U,Zr)O_2$ ceramic melt from throughout the core exhibited regions of single-phase solid solution and regions of uranium- and zirconium-rich oxide phases. X-ray diffraction measurements confirmed the presence of the cubic $(\underline{U},Zr)O_2$ phases and both tetragonal and monoclinic $(\underline{Zr},U)O_2$ phases. The presence of single-phase regions indicates that portions of the $(U,Zr)O_2$ melt were rapidly quenched, whereas the presence of two-phase regions indicates that other portions of the melt cooled more slowly. In particular, the presence of monoclinic $(\underline{Zr},U)O_2$ indicates a thermal hold below approximately 1400 K to allow a phase transformation from tetragonal to monoclinic structures. These microstructures are consistent with reflood water coming into direct contact and rapidly quenching some of the ceramic melt, with other regions taking much longer to cool due to the large thermal mass and the inability of water to come in direct contact with much of the material. These data are also consistent with thermocouple data, which indicate that elevated temperatures existed for several days following core reflood.

The microstructure of the ceramic melt that relocated to the lower plenum provides an indication of how this material may have flowed over the stainless steel flow distributor and the stainless steel liner covering the lower vessel head without damaging these materials. These stainless steel materials melt at approximately 1720 K, whereas molten $(U,Zr)O_2$ requires temperatures in excess of 2810 K. However, the ceramic melt contained spinel structures in the grain boundaries and around gas voids in the solidified structure, which were composed of (Fe,Cr)-oxides that could be liquid at temperatures below the

melting point of the stainless steel. The presence of spinels in these locations also indicates that these were the last materials to solidify. The material at this point in its descent to the lower plenum may therefore have been transported as a two-phase solid-liquid mass, with the liquid spinel carrying the solidified $(U,Zr)O_2$.

Despite the complex mixtures of molten materials present in TMI-2, general trends were observed in the segregation of various elements in the previously molten regions. This information provides an indication of the material interactions that did occur, and in particular, the low temperature liquefaction of materials below their melting points that leads to early material relocation. Mixtures of zirconium with iron and nickel indicate that Zr-Fe and Zr-Ni eutectic interactions resulted in the liquefaction of stainless steel cladding and Inconel spacer grids at temperatures below their melting points (~1720 K). Phase diagram examinations by Kleykamp and (see Reference 26) have shown that active zirconium-steel/Inconel eutectic interactions can occur at temperatures as low as 1220 K in both cases, with the kinetics becoming much more rapid from 1400-1500 K. TMI-2 also contained Al_2O_3-B_4C poison rods surrounded by zircaloy cladding, and Zr-Al-O eutectic interactions can lead to liquefaction of these materials above approximately 1620 K (see Appendix B). These materials were found in the central melt regions and in the solidified crust; this indicates that such reactions could have lead to the early failure of TMI-2 fuel assemblies containing these poison rods. It was observed that in adjacent fuel assemblies containing control rods and burnable poison rods, the fuel assembly with the burnable poison rod suffered greater damage (see Reference 28).

Silver-zirconium eutectic interactions can also lead to low temperature liquefaction of the zircaloy cladding above 1200 K, and such reactions were definitely observed in the LOFT FP-2 experiment, but very little of this type of material was observed in TMI-2. Core pressures may have been a factor in the mode of silver release from the control rods (aerosol or liquid would be favored at relatively low and high core pressures, respectively), which could affect the extent of this type of interaction. LOFT FP-2 was conducted under low-pressure conditions (less than 200 psi), whereas pressures in the TMI-2 core were much higher.

The examinations of TMI-2 materials also indicate that molten zircaloy was responsible for the liquefaction of fuel, and that large amounts of $(U,Zr)O_2$ ceramic melt were formed during the accident. The liquefaction of the fuel by molten zircaloy can take place at temperatures as low as approximately 2000 K, with molten $(U,Zr)O_2$ requiring temperatures in excess of 2810 K.

The oxidation state of the melts also provides an indication of the oxygen potential in the core during the accident. Metallic melts were commonly composed of Ag-In and Fe-Ni-Sn, with other elements such as Zr, Cr, and Cd also present in lesser amounts in a multitude of compositional variations. Oxidized phases commonly contained U, Zr, Cr, Al, and Fe. As previously discussed in Section 5, this indicates an oxygen potential of approximately -150 kJ/mole at 2273 K to -500 kJ/mole at 1473 K.

Examination of partially intact fuel assembly remnants on the periphery of the core indicates that the most severe damage was limited to the central and upper regions of the core, from which material relocated to the lower plenum. Despite the extent of the damage and the relocation of tons of hot molten material from the core region, TMI-2 demonstrated that such an accident can be terminated without the loss of the integrity of the reactor vessel or containment.

7. SUMMARY AND CONCLUSIONS

A multitude of examinations were conducted by several investigators at different laboratories around the world on samples from throughout the damaged TMI-2 reactor core. The results of all these examinations could be interrelated to provide a more complete understanding of the TMI-2 accident, and the consistency of the overall findings provides a measure of the confidence in the experimental results. This section summarizes the major results of all these examinations.

The stratification of relocated material was similar to the stratification observed in severe fuel damage experiments. Metallic melts were the first to relocate and eventually form the lower crust. Above the lower crust was a region consisting primarily of $(U,Zr)O_2$ ceramic melt. The upper crust was also composed of a matrix of ceramic melt, but it also had agglomerations of metallic melt that had penetrated into the solidifying crust. A debris bed of fuel and cladding fragments and molten materials rested on top of the upper crust.

Metallic melts found throughout the core largely consisted of various Fe-Ni-Sn and Ag-In alloys with other minor elements mixed in. The ceramic melts were mostly $(U,Zr)O_2$ with spinels of the type $FeCr_2O_4$ in the grain boundaries and adjacent to steam gas bubbles.

The melt that relocated to the lower plenum was similar to that found in the central melt region: $(U,Zr)O_2$ ceramic melt with small amounts of spinel material. This relocated material did not significantly damage the stainless steel flow distributor nor the stainless steel liner on the lower vessel head. This suggests that the melt temperature was low enough to allow rapid cooling at the interface with the steel, so that the 1720 K melting point of the stainless steel was not exceeded when it came in contact with these materials. The microstructure of the solidified melt suggests that two-phase solid-liquid mass transport occurred for the latter part of the descent in the lower vessel, with the spinel acting as a lubricant for the solidified $(U,Zr)O_2$ phase. Temperatures in excess of 2800 K would have been required for the $(U,Zr)O_2$ phase to become molten.

Metallographic examinations of the ceramic melts revealed that they consisted of single-phase solid solutions of $(U,Zr)O_2$, as well as separate phases of uranium-rich $(U,Zr)O_2$ and zirconium-rich $(Zr,U)O_2$. X-ray and neutron diffraction confirmed the presence of the cubic $(U,Zr)O_2$ structure, as well as both tetragonal and monoclinic $(Zr,U)O_2$. This indicates that some melt material was rapidly quenched so that the single-phase solid solution was retained, whereas other regions of the ceramic melt cooled more slowly, allowing the formation of the two-phase structure. Thermal holds below approximately 1900 K would be required to form the two-phase structures with tetragonal $(Zr,U)O_2$, with thermal holds below approximately 1400 K to form the two-phase structure with monoclinic $(Zr,U)O_2$. This is consistent with some portions of the ceramic melt coming into direct contact with reflood water, whereas other portions of the melt were shielded and took much longer to cool. Thermocouple measurements indicated that much of the core remained at elevated temperatures for several days after the core was reflooded.

The presence of Zr-Fe and Zr-Ni melts suggests that liquefaction of stainless steel cladding and Inconel spacer grids occurred during the TMI-2 accident. These types of liquefaction processes have been observed in many severe fuel damage experiments, and this behavior may have been largely responsible for the early relocation of metallic melts and the formation of the metallic lower crust.

Elements generally found in the metallic state were Ag, In, Cd, Ni, Sn, and Fe. Elements generally found in the oxidized state were U, Zr, Cr, Al, and Fe. Comparison with an Ellingham diagram suggests oxygen potential of -150 kJ/mole at 2000°C and -500 kJ/mole at 1200°C.

Radionuclide examinations performed on the CSNI samples provided information on the chemical behavior of a number of the principal fission products. One specific observation of importance is that the radionuclides of Mo, Ru, and Tc are correlated among each other and with Fe and Ni. Therefore, the noble fission metals can be expected to concentrate in metallic phases and would be expected to be primarily concentrated in the crust regions and in metallic inclusions in the core. Another important observation is that there is a correlation between the rare earth fission product Sr and a structural

material. La, Pr, Ce, Nd, Pm, and Sr are more significantly correlated with Zr than with U, which suggests that these lanthanides may prefer, as host lattice, the Zr-rich tetragonal $(Zr,U)O_2$ phase rather than cubic uranium-rich phases. These data suggest that many of the relatively low volatility radionuclides are relatively mobile within the fuel melt and are not fully retained in the uranium matrix as might be expected.

8. REFERENCES

1. E. L. Tolman et al., *TMI-2 Accident Scenario Update*, EGG-TMI-7489, December 1986.

2. G. R. Eidem et al., "TMI-2 Defueling Conditions and Summary of Research Findings," *Proceedings of IAEA/NEA International Symposium on Severe Accidents in Nuclear Power Plants, Sorrento Italy, March 21-25, 1988.*

3. J. Adams and R. Smith, *Lower Plenum Video Data Survey*, EGG-TMI-7429, July 1987.

4. E. L. Tolman et al., *TMI-2 Accident Evaluation Program*, EGG-TMI-7048, September 1986.

5. M. L. Russell et al., *TMI-2 Accident Evaluation Program Sample Acquisition and Examination Plan for FY-1987 and Beyond*, EGG-TMI-7521, February 1987.

6. E. L. Tolman et al., *TMI-2 Core Bore Acquisition Summary Report*, Rev. 1, EGG-TMI-7385, February 1987.

7. D. W. Akers et al., *The TMI-2 Lower Core Region: Examination and Analysis Vols. 1 and 2*, GEND-INF-092, August 1989.

8. M. L. Russell et al., *TMI-2 Accident Evaluation Program Sample Acquisition and Examination Plan for FY-1988 and Beyond*, EGG-TMI-7992, February 1988.

9. B. G. Schnitzler and J. B. Briggs, *TMI-2 Isotopic Inventory Calculations*, EGG-PBS-6798, August 1985.

10. Nuclear Safety Analysis Center, *TMI-2 Accident Core Heat-Up Analysis*, NSAC-25, June 1981.

11. C. V. McIsaac and D. W. Akers, *TMI-2 Core Bore Gamma-Ray Spectroscopy Measurements*, EGG-TMI-8058, June 1988.

12. P. Hofmann et al., "Reactor Core Material Interactions at Very High Temperatures," *Nuclear Technology*, Vol. 87, August 1989, pp. 146-186 (see Appendix B).

13. S. M. Jensen et al., *Postirradiation Examination Data and Analyses for OECD LOFT Fission Product Experiment LP-FP-2*, Vols. 1 and 2, OECD-LOFT-T-3810, December 1989.

14. D. A. Petti et al., *Power Burst Facility (PBF) Severe Fuel Damage Test 1-4 Test Results Report*, NUREG/CR-5163, EGG-2542, April 1989.

15. S. M. Jensen and D. W. Akers, "Postirradiation Examination Results from the LP-FP-2 Center Fuel Module," *Proceedings of the Final OECD/LOFT Meeting, Madrid, Spain, May 1990*, to be published.

16. M. L. Carboneau, "Highlights of the OECD/LOFT LP-FP-2 Experiment, Including Hydrogen Generation, Fission Product Chemistry, and Transient

Fission Product Release Fractions," *Proceedings of the Final OECD/LOFT Meeting, Madrid, Spain, May 1990*, to be published.

17. S. M. Modro and M. L. Carboneau, "The Severe Fuel Damage Scenario. Discussion of the Relative Influence of the Transient and Reflood Phase in Affecting the Final Condition of the Bundle," *Proceedings of the Final OECD/LOFT Meeting, Madrid, Spain, May 1990*, to be published.

18. R. Hobbins and G. D. McPherson, "A Summary of Results from the LOFT LP-FP-2 Test and Their Relationship to Other Studies at the Power Burst Facility and of the Three Mile Island Unit 2 Accident," *Proceedings of the Final OECD/LOFT Meeting, Madrid, Spain, May 1990*, to be published.

19. M. L. Carboneau et al., *Experiment Analysis and Summary Report for OECD/LOFT Project Fission Product Experiment LP-FP-2*, OECD/LOFT-T-3806, June 1989.

20. M. L. Carboneau et al., *OECD/LOFT Fission Product Experiment LP-FP-2 Data Report*, OECD/LOFT-T-3805.

21. D. S. Cox et al., Examination of TMI-2 Core Samples in Canada, Atomic Energy of Canada Limited (see Appendix C).

22. M. Trotabas et al., *TMI-2 Core Materials Examinations at Commissariat A L' Energie Atomique*, SEMCI-89-DT-667, December 1989 (see Appendix D).

23. G. Bart et al., *TMI-2 Core Sample Evaluation at PSI (Paul Scherrer Institute)*, TM-43-90-07, February 1990 (see Appendix E).

24. A. J. Manley et al., *Examination of TMI-2 Core Material*, PWR-TMI2-P(90)91, March 1990 (see Appendix F).

25. P. Bottomley and M. Coquerelle, Final Report of the Metallurgical Examination of Samples Extracted From the Damaged TMI-2 Reactor Core, Commission of the European Communities, Joint Research Centre, January 1990 (see Appendix G).

26. H. Kleykamp and R. Pejsa, Elemental and Structural Analysis on Selected Samples From TMI-2 Core, Further Preliminary Results, Kernforschungszentrum Karlsruhe, Final Meeting at Tokyo, 21-25 May 1990 (see Appendix H).

27. A. Brown et al., "Analysis of Crystalline Phases in Core Bore Materials From Three Mile Island Unit 2," *Nuclear Technology*, Vol. 87, August 1989, pp. 137-145 (see Appendix I).

28. *Proceedings of the First International Information Meeting on the TMI-2 Accident, Germantown, Maryland, October 21, 1985*, CONF-8510166, U.S. Nuclear Regulatory Commission (1985).

29. L. A. Neimark et al., "Fuel Relocation Mechanisms Based on Microstructures of Debris," *Nuclear Technology*, Vol. 87, August 1989, pp. 187-190 (see Appendix J).

30. C. S. Olsen et al., "Materials Interactions and Temperatures in the Three Mile Island Unit 2 Core," *Nuclear Technology*, Vol. 87, August 1989, pp. 57-94.